THE JOURNAL OF BIOLOGICAL CHEMISTRY VOL. 287, NO. 44, pp. 36732–36743, October 26, 2012

Molecular Plasticity Regulates Oligomerization and Cytotoxicity of the Multipeptide-length Amyloid-β Peptide Pool*[S]

Received for publication, June 22, 2012, and in revised form, September 4, 2012 Published, JBC Papers in Press, September 19, 2012, DOI 10.1074/jbc.M112.394635

Annelies Vandersteen[‡§¶‖], Marcelo F. Masman[‡‡1], Greet De Baets[‡§¶], Wim Jonckheere[‡¶], Kees van der Werf[‖], Siewert J. Marrink[‡‡], Jef Rozenski[§§], Iryna Benilova[¶¶], Bart De Strooper[¶¶], Vinod Subramaniam[‖], Joost Schymkowitz[‡§], Frederic Rousseau[‡§], and Kerensa Broersen[¶‖2]**

From the [‡]Switch Laboratory, Flanders Institute for Biotechnology (VIB), B-3000 Leuven, Belgium, the [§]Department of Molecular Cell Biology, K.U. Leuven, B-3000 Leuven, Belgium, [¶]Structural Biology, Flanders Institute for Biotechnology (VIB) and Vrije Universiteit Brussel (VUB), B-1050 Brussels, Belgium, [‖]Nanobiophysics group, MIRA Institute for Biomedical Technology and Technical Medicine and MESA+ Institute for Nanotechnology, University of Twente, 7500 AE Enschede, The Netherlands, [**]Department of Molecular Neurobiology, University of Groningen, 9747 AG Groningen, The Netherlands, [‡‡]Groningen Biomolecular Sciences and Biotechnology Institute and Zernike Institute for Advanced Materials, University of Groningen, 9747 AG Groningen, The Netherlands, [§§]Laboratory of Medicinal Chemistry, Rega Institute for Medical Research, B-3000 Leuven, Belgium, and [¶¶]VIB Center for Biology of Disease, Flanders Institute for Biotechnology (VIB) and Center for Human Genetics, K.U. Leuven, B-3000 Leuven, Belgium

Background: Aβ peptide, implicated in Alzheimer disease, occurs in various lengths.
Results: Non-abundant $A\beta_{1-38}$ and $A\beta_{1-43}$ affect oligomerization, cytotoxicity, and aggregation of $A\beta_{1-40}$ and $A\beta_{1-42}$.
Conclusion: Small amounts of Aβ lengths other than $A\beta_{1-40}$ or $A\beta_{1-42}$ significantly alter the behavior of the total Aβ pool.
Significance: Drug strategies targeting APP processing to affect $A\beta_{1-38}$ levels need careful consideration.

Current therapeutic approaches under development for Alzheimer disease, including γ-secretase modulating therapy, aim at increasing the production of $A\beta_{1-38}$ and $A\beta_{1-40}$ at the cost of longer Aβ peptides. Here, we consider the aggregation of $A\beta_{1-38}$ and $A\beta_{1-43}$ in addition to $A\beta_{1-40}$ and $A\beta_{1-42}$, in particular their behavior in mixtures representing the complex *in vivo* Aβ pool. We demonstrate that $A\beta_{1-38}$ and $A\beta_{1-43}$ aggregate similar to $A\beta_{1-40}$ and $A\beta_{1-42}$, respectively, but display a variation in the kinetics of assembly and toxicity due to differences in short timescale conformational plasticity. In biologically relevant mixtures of Aβ, $A\beta_{1-38}$ and $A\beta_{1-43}$ significantly affect the behaviors of $A\beta_{1-40}$ and $A\beta_{1-42}$. The short timescale conformational flexibility of $A\beta_{1-38}$ is suggested to be responsible for enhancing toxicity of $A\beta_{1-40}$ while exerting a cyto-protective effect on $A\beta_{1-42}$. Our results indicate that the complex *in vivo* Aβ peptide array and variations thereof is critical in Alzheimer disease, which can influence the selection of current and new therapeutic strategies.

Extracellular deposits containing the amyloid-β peptide (Aβ)[3] represent one of the hallmarks of Alzheimer disease (AD) (1). Aβ is generated from the transmembrane amyloid precursor protein (APP) by β- and γ-secretase-mediated cleavage (2–4). This action primarily results in the production of the 40-amino acid $A\beta_{1-40}$ peptide and smaller amounts of the 42-amino acid $A\beta_{1-42}$ peptide in addition to minute quantities of other Aβ peptides ranging in length from 27 to 43 amino acids (5, 6). The observed variation at the Aβ C terminus is a consequence of the heterogeneous γ-secretase processing pattern (7) that first generates $A\beta_{1-48}$ and $A\beta_{1-49}$ peptides through cleavage of APP at the ϵ-site followed by successive trimming of every three to four residues (8, 9). Hence, the preferential $A\beta_{1-40}$ production pathway involves the intermediate formation of $A\beta_{1-43}$, $A\beta_{1-46}$, and $A\beta_{1-49}$ (10). The array of Aβ peptides that is produced in this way can be affected by clinical mutations in APP (8, 11) or in the presenilin-1 active site subunit of the γ-secretase complex (8, 11, 12). Mutations of presenilin-1 potently shift the ϵ-cleavage site on APP toward the $A\beta_{1-38}$ production pathway with intermediate formation of $A\beta_{1-42}$, $A\beta_{1-45}$, and $A\beta_{1-48}$ (10).

Generally, longer Aβ peptides are more hydrophobic as the C termini progressively form part of the transmembrane domain of APP and are, therefore, considered more aggregation-prone (13–15). Consistent with this finding, senile plaques have been found to be primarily composed of $A\beta_{1-42}$ and $A\beta_{1-43}$, whereas shorter Aβ peptides remain largely undetected (16–

* This work was supported by the Agency for Innovation by Science and Technology in Flanders (IWT), a project grant from the "Stichting voor Alzheimer Onderzoek" (SAO), an Odysseus grant from the National Funds for Scientific Research Flanders (FWO), an Alzheimer Research UK (ARUK) grant, and a European Molecular Biology Organization Short-term Fellowship.
[S] This article contains supplemental Experimental Procedures and Figs. 1–4.
[1] A fellow post-doc of the Brain Foundation of the Netherlands (Hersenstichting Nederland).
[2] To whom correspondence should be addressed: Faculty of Science and Technology, Nanobiophysics, MIRA Institute for Biomedical Technology and Technical Medicine, University of Twente, 7500 AE Enschede, The Netherlands. Tel.: 31(0)534893655; Fax: 31(0)534891105; E-mail: k.broersen@utwente.nl.

[3] The abbreviations used are: Aβ, amyloid-β peptide; AD, Alzheimer disease; APP, amyloid precursor protein; GSM, γ-secretase modulator; ThT, thioflavin T; AFM, atomic force microscopy; MD, molecular dynamics; DSSP, definition of secondary structure of proteins.

18). Based on these observations, γ-secretase inhibitors were developed that aimed at lowering the activity of γ-secretase and reducing Aβ production. However, the multifunctionality of the γ-secretase enzyme, including a critical role in the Notch signaling process, led to the recognition that total inhibition of this enzyme is an undesired approach. This observation served as a starting point for the generation of γ-secretase modulators (GSMs) that fine-tune the action of γ-secretase to shift the production of Aβ peptides toward shorter variants while leaving the total Aβ peptide production and activity of γ-secretase unchanged (19, 20). Given the finding that specifically aggregated Aβ peptide can lead to a neurotoxic response, GSMs offered in this way a promising perspective as a potential agent to slow down the progress of senile plaque deposition in AD by decreasing the production of $A\beta_{1-42}$ while increasing that of $A\beta_{1-38}$. The first generation of GSMs was classified as non-steroidal anti-inflammatory drugs and derivatives thereof. Administration of these drugs to healthy individuals showed positive effects on cognitive function that could be entirely attributed to the cyclo-oxygenase (COX) inhibitory action of the compound without displaying GSM action (21, 22). Clinical trials with non-COX inhibitory non-steroidal anti-inflammatory drugs did not display protective effects on AD disease progress, possibly as a result of the low potency and poor brain penetrance of the compounds, inhibition of Notch processing, or accumulation of APP C-terminal fragments (23). A next generation of Notch-sparing GSMs and non-steroidal anti-inflammatory drug-derived compounds with improved potency and brain penetration are currently being developed but yet await clinical trials (22).

The reported neurotoxicity of $A\beta_{1-43}$ (12) as well as the observed increasing (24) and decreasing $A\beta_{1-38}$ (25) levels in cerebrospinal fluid upon AD progress, indicate that the contributions of $A\beta_{1-38}$ and $A\beta_{1-43}$ to AD progression require further elucidation. By comparing their pathogenicity, aggregation profiles, and biophysical properties with that of well studied $A\beta_{1-40}$ and $A\beta_{1-42}$, we show that $A\beta_{1-38}$ and $A\beta_{1-43}$ both form aggregates that differ in cytotoxic potential. We further show that inclusion of $A\beta_{1-38}$ and $A\beta_{1-43}$ into complex mixtures containing $A\beta_{1-40}$ and $A\beta_{1-42}$ substantially affects the behavior of total Aβ and that $A\beta_{1-38}$ and $A\beta_{1-40}$, previously considered non-amyloidogenic, can unexpectedly become toxic in these mixtures. These findings have been related to conformational plasticity of the respective peptides and highlight the relevance of understanding the role of C-terminal variation of Aβ peptides and their potential as therapeutic targets.

EXPERIMENTAL PROCEDURES

Preparation of Aβ Peptides and Peptide Ratios—Aβ peptides (rPeptide) were dissolved and mixed as described before (26, 27). Briefly, Aβ was dissolved into 1,1,1,3,3,3-hexafluor-2-propanol, evaporated with an N_2 stream, and redissolved in dimethyl sulfoxide. Solvents were removed by elution over a 5-ml HiTrap desalting column (GE Healthcare) into a 50 mM Tris buffer, pH 7.4, containing 1 mM EDTA. Peptide concentrations were measured using the Coomassie (Bradford) Protein Assay kit (Thermo Scientific) against a bovine serum albumin standard (Thermo Scientific). Aβ peptide concentrations were diluted to a concentration of 50 μM in 50 mM Tris buffer, pH 7.4, containing 1 mM EDTA and incubated at 25 °C under quiescent conditions for further experiments.

Thioflavin T Fluorescence—Fibrillation kinetics of Aβ in the presence of 12 μM thioflavin T (ThT) were followed *in situ* at 25 °C using a Fluostar OPTIMA fluorescence plate reader (BMG LABTECH GmbH) at an excitation wavelength of 440 nm and an emission wavelength of 480 nm. Readings were recorded in triplicate every 5 min for a period of 10 h and corrected by subtracting the intensity obtained for buffer containing 12 μM ThT. The end of the lag phase was determined manually. Elongation rate was fitted to the central region of the exponential phase. Final fluorescence was determined at 10 h of incubation.

Dot Blot—At various time points a volume of 5-μl sample was spotted onto Protran BA85 nitrocellulose blotting membrane (Whatman). The membranes were blocked at 25 °C in phosphate-buffered saline containing 0.2% Tween 20 (PBST XL) for 1 h and incubated for 1 h at 25 °C with primary rabbit polyclonal anti-oligomer antibody (A11) (Invitrogen), diluted 1:4000 in 100 mM Hepes, pH 7.0 (28). After incubation with secondary anti-rabbit-HRP-tagged antibody (Promega) diluted 1:5000 in phosphate-buffered saline containing 0.05% Tween 20 (PBST) for 0.5 h at 25 °C, the membranes were visualized using the Immobilon™ Western chemiluminescent HRP substrate system (Millipore).

Transmission Electron Microscopy—A volume of 5 μl of Aβ was adsorbed to carbon-coated Formvar film on 400-mesh copper grids (Agar Scientific Ltd) for 1 min. The grids were washed in ultrapure water (Merck) and stained with 1% (w/v) uranyl acetate (VWR). Samples were studied using a JEOL JEM-2100 microscope at an accelerating voltage of 200 kV or a JEOL JEM-1400 microscope at an accelerating voltage of 80 kV (JEOL Ltd.).

Atomic Force Microscopy (AFM)—AFM imaging was performed on a custom-built instrument using Si_3N_4 tips (Veeco Instruments, Woodbury NY; type MSCT-AUHW) with a spring constant of 0.5 newtons/m and a nominal tip radius of 10 nm. The measurements were made in tapping mode in air, with a tapping amplitude of less than 4 nm. The AFM scan settings were optimized to minimum force interaction with the sample. AFM samples were prepared by placing 5 μl of sample on freshly cleaved mica. After 4 min adsorption time, unbound Aβ was washed off twice with 100 μl of ultrapure water (Merck) and dried using a gentle N_2 stream. The images are represented in three-dimensions after removal of height discontinuities between subsequent scan lines and compensation for piezo drift using SPIP software (Image Metrology A/S, Lyngby, Denmark).

Far-UV Circular Dichroism (CD)—After 1.5 h of incubation, Aβ was diluted to 15 μM and placed in a quartz cuvette with an optical path of 3 mm, and far-UV circular dichroism spectra were recorded in a Jasco J-715 spectrometer. The wavelength range was set from 260 to 190 nm with 0.2-nm resolution, 2.0-s response time, 2.0-nm bandwidth at a scanning speed of 50 nm/min. Data were collected as averages of eight scans. The spectra obtained were corrected by subtracting the spectrum obtained for buffer only.

Attenuated Total Reflection Fourier Transform Infrared Spectroscopy (ATR FTIR)—Using a Bruker Tensor 27 infrared spectrophotometer equipped with a Bio-ATR II accessory, infrared spectra of aggregating Aβ (220 μM, 25 °C, in 50 mM Tris buffer, pH 7.4, containing 1 mM EDTA) were recorded. The samples were applied to the FTIR sample holder and incubated for 1.5 h. Spectra were recorded in the range of 900–3500 cm^{-1} at a spectral resolution of 4 cm^{-1} at the beginning (time 0) and the end (time 1.5 h) of the experiment. Each measurement consisted of 120 accumulations. The spectrophotometer was continuously purged with dried air. The obtained spectra were corrected for atmospheric interference, baseline-subtracted, and rescaled in the amide I area (1700 to 1600 cm^{-1}). Changes of secondary structure over 1.5 h of incubation were analyzed by subtraction of the spectrum recorded at time 0.

In Silico Predictions—The statistical mechanics algorithm TANGO (29) was used to predict aggregation-prone regions in the Aβ peptide sequence (30). TANGO provides an aggregation propensity (0–100%) per residue as output. An aggregating region is defined as a continuous stretch of residues with an individual TANGO score higher than 5% and a total score for the region higher than 50%. Total TANGO scores are calculated as the sum of the individual residual TANGO scores for a given sequence. TANGO calculations were performed using the online TANGO calculator with the following parameters: pH of 7.0, a temperature of 298.15 K, and 0.02 M ionic strength without N- or C- terminal protection.

Molecular Dynamics (MD) Simulations—The NMR structure (Protein Data Bank entry 1IYT) was used as starting structure of $A\beta_{1-42}$ and as a template to generate the other Aβ species studied here. All MD simulations were performed with GROMACS 4.5.3 using the OPLS/AA force field (31). Experimental details are described in the supplemental materials. The LINCS algorithm (32) was used for bond-length constraining. The non-bonded pair list was updated every 10 fs. The simulation of each system was repeated at least 10 times and then individually analyzed, and their averaged properties are reported here. Programs included in the GROMACS package as well as some in-house scripts were used to perform the analysis of the trajectories. Molecular graphics images were produced using the UCSF Chimera package from the Resource for Biocomputing, Visualization, and Informatics at the University of California, San Francisco (supported by National Institutes of Health Grant P41 RR001081) (33).

Neuroblastoma Cells and Cytotoxicity—All tissue culture reagents were obtained from Invitrogen. The human neuroblastoma cell line SH-SY5Y (ATCC number CRL-2266) was cultured in DMEM/F-12 supplemented with 10% fetal bovine serum (HyClone, ThermoScientific). The cells were incubated at 37 °C in a humidified 5% CO_2 atmosphere. Cytotoxicity assays were performed in 96-well plates after plating 25,000 cells per well in serum-deprived DMEM/F-12. After pre-aggregation for 1.5 h, Aβ was diluted in DMEM/F-12 and added to the cells. After 24 h of treatment, cell viability was analyzed using the Cell Titer Blue Cell Viability assay (Promega). After 4 h, color conversion was analyzed by measuring the fluorescence intensity of the samples at an excitation wavelength of 544 nm and an emission wavelength of 590 nm using a Fluostar OPTIMA fluorescence plate reader. Values are percent of cell viability ± S.D., and buffer signal was normalized to 100%.

Statistical Analysis—Results from ThT fluorescence and cytotoxicity experiments were analyzed using two-tailed unpaired *t* tests for significance. Significance is indicated by *** ($p < 0.0001$), ** ($p < 0.0005$), and * ($p < 0.005$). MD results were analyzed using two-way analysis of variance with repeated measures to determine whether each group differs significantly from each other and multivariate analysis to determine at which specific point the groups significantly differed. Bonferroni post hoc analysis was applied. Significance is indicated by ## ($p < 0.005$). All properties determined by MD techniques are reported as the average property of 10 simulations ± S.E.

RESULTS

Aβ Peptide Length Determines Aggregation, Oligomerization, and Toxicity—It has been reported before that $A\beta_{1-40}$ and $A\beta_{1-42}$ display different aggregation kinetics (13, 34). Consistent with these data, we also observed substantial differences in aggregation kinetics as a function of peptide length (Fig. 1*A*) when comparing $A\beta_{1-38}$, $A\beta_{1-40}$, $A\beta_{1-42}$, and $A\beta_{1-43}$ using ThT fluorescence. Although $A\beta_{1-38}$ and $A\beta_{1-40}$ showed a delayed onset of aggregation, $A\beta_{1-42}$ and $A\beta_{1-43}$ rapidly aggregated, as suggested by the immediate rise in ThT fluorescence signal. Even though the aggregation regimes of $A\beta_{1-38}$ and $A\beta_{1-40}$ are generally alike, with a distinct lag phase and significant and sigmoidal development of ThT signal after 10 h of incubation, $A\beta_{1-38}$ showed a more rapid onset of aggregation compared with $A\beta_{1-40}$. The final (10 h) ThT fluorescence intensity of both $A\beta_{1-42}$ and $A\beta_{1-43}$ aggregates was very low compared with $A\beta_{1-38}$ and $A\beta_{1-40}$ (Fig. 1*B*) and has been reported to correlate with the weight concentration and the morphology of the formed fibrils (35). Transmission electron microscopy showed that 0.5 h of incubation of $A\beta_{1-42}$ and $A\beta_{1-43}$ resulted in networks of intertwined fibrils, whereas for $A\beta_{1-38}$ and $A\beta_{1-40}$ aggregates were absent (Fig. 1*C*). Upon incubation for 4 h, the fibrillar network observed for $A\beta_{1-43}$ had progressed into polymorphous clusters interconnected by mature fibrils. $A\beta_{1-42}$ showed a similar organization, yet short and aligned fibrils seemed more prevalent compared with $A\beta_{1-43}$. In contrast, $A\beta_{1-38}$ and $A\beta_{1-40}$ both formed long, negatively stained and regularly twisted fibrils with a diameter of 8–12 nm that is typically observed for amyloid-like fibrils (36). All Aβ peptides formed extensive fibrillar networks upon incubation for 24 h. To establish by which mechanism C-terminal variation affected the observed aggregation characteristics of Aβ, the statistical thermodynamics algorithm TANGO was used to predict aggregating stretches in the various Aβ peptides tested. TANGO scores further showed that, in general, increasing aggregation propensity could be observed with increasing peptide length with the exception of Aβ varying in length from 37 to 40 amino acids (Fig. 1*D*). A per-residue analysis of the aggregation propensity showed that all Aβ sequences contain a common aggregating stretch ranging from residue 16 to residue 22 (37) (Fig. 1*E*). A second aggregating region starts at residue 28 and spans the remaining C-terminal part of the sequence and showed strong variation with Aβ length due predominantly to the presence of two subsequent glycine residues, which disfavor

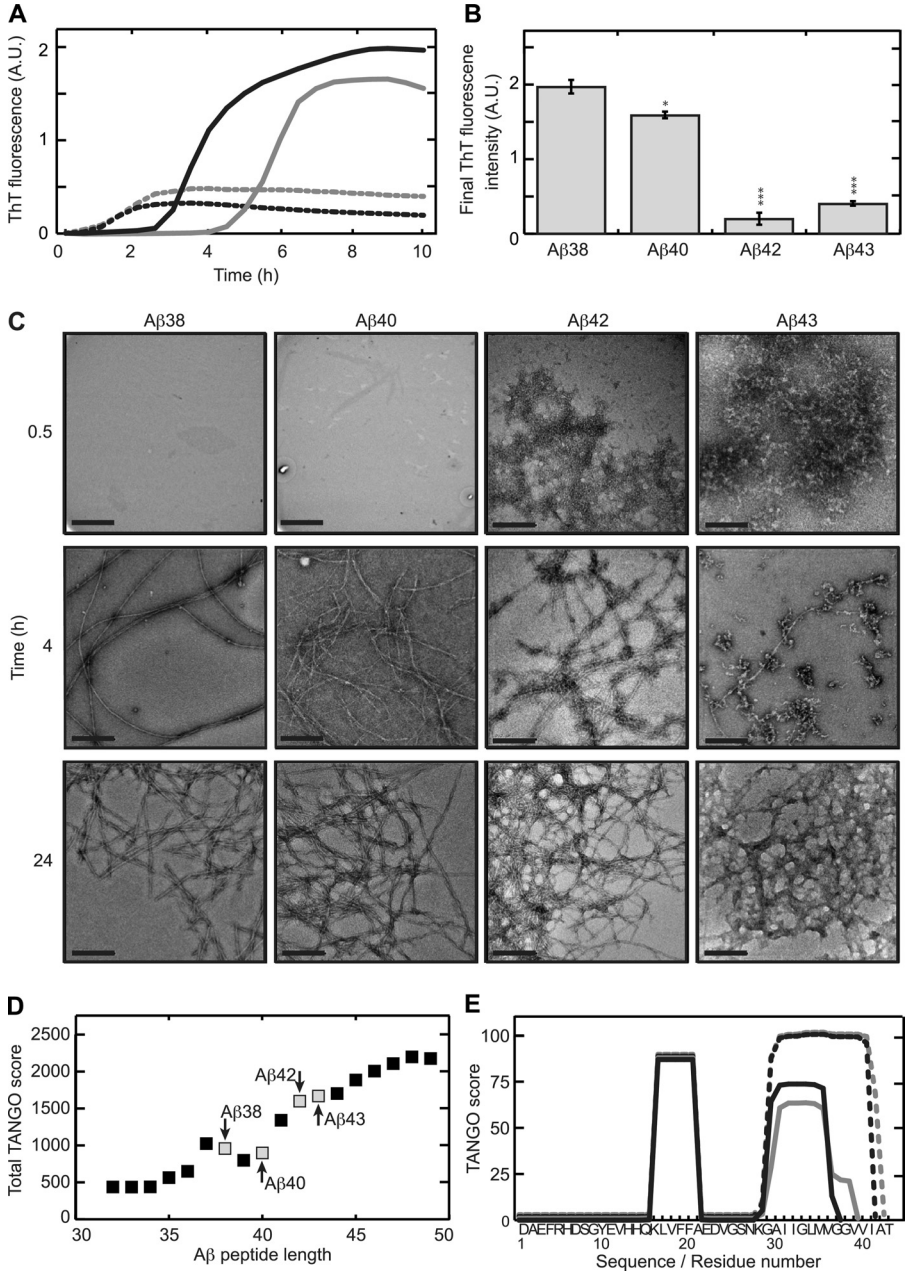

FIGURE 1. **C-terminal heterogeneity affects aggregation kinetics of the Aβ peptide.** *A*, ThT fluorescence was recorded *in situ* every 5 min at 25 °C. $A\beta_{1-38}$ (*continuous black line*) and $A\beta_{1-40}$ (*continuous gray line*) display a lag phase, whereas $A\beta_{1-42}$ (*dotted black line*) and $A\beta_{1-43}$ (*dotted gray line*) induce ThT fluorescence almost immediately. The values represent the means of three experiments. *A.U.*, absorbance units. *B*, final (10 h) ThT fluorescence intensities was derived from *panel A*. Statistical significance (unpaired 2-tailed *t* test) compared with the $A\beta_{1-38}$ value is indicated by *** ($p < 0.0001$), ** ($p < 0.0005$), or * ($p < 0.005$). *C*, after 0.5 h of incubation $A\beta_{1-42}$ and $A\beta_{1-43}$ formed networks, whereas $A\beta_{1-38}$ and $A\beta_{1-40}$ do not show visible aggregates. After 4 h of incubation, $A\beta_{1-38}$ and $A\beta_{1-40}$ formed 8–12-nm wide, extended, negatively stained fibrils. $A\beta_{1-42}$ organized into a network of rigid 14–16-nm wide fibrils. For $A\beta_{1-43}$, a mixture of protofibrils and fibrils was observed. After 24 h all Aβs formed similar fibrillar networks. *Scale bar*, 200 nm. *D*, total TANGO scores indicated an increasing overall aggregation propensity of Aβ with increasing peptide length. 37–40 amino acid-long peptides deviated from this trend. Peptides studied in this manuscript are marked. *E*, sequence-based prediction of aggregation prone stretches by the TANGO algorithm suggests a common aggregating region in the core of the peptide and a second aggregating region at the C terminus. Differences in total TANGO score (*D*) are exclusively due to the C-terminal aggregating region. $A\beta_{1-38}$ (*continuous black line*) and $A\beta_{1-40}$ (*continuous gray line*) display similar predicted aggregation propensity, whereas that of $A\beta_{1-42}$ (*dotted black line*) and $A\beta_{1-43}$ (*dotted gray line*) were higher.

aggregation but which are compensated by additional aggregation promoting residues in the longer forms. Our analysis shows that differences in aggregation propensity directly stem from C-terminal variation. In line with our observation that $A\beta_{1-38}$ aggregates faster than $A\beta_{1-40}$ (Fig. 1*A*), TANGO predicted a slightly higher aggregation propensity for $A\beta_{1-38}$ than for $A\beta_{1-40}$ (Fig. 1, *D* and *E*).

ThT does not interact strongly with oligomeric Aβ (38), whereas soluble oligomeric Aβ is generally considered to represent the toxic species (39–41). We used complementary oligomer-sensitive techniques such as the A11 oligomer-specific antibody (28) and AFM to obtain information on the lifetime of oligomeric Aβ as a function of C-terminal variation. Aβ peptides were allowed to aggregate and were tested for A11 reac-

tivity at various time points of incubation (Fig. 2*A*). $A\beta_{1-42}$ and $A\beta_{1-43}$ formed A11-positive oligomers already after 0.5 h of incubation, whereas $A\beta_{1-38}$ and $A\beta_{1-40}$ only interacted with the A11-antibody after an incubation time of 5 and 6 h, respectively, with $A\beta_{1-38}$ exhibiting substantially stronger staining with the antibody than $A\beta_{1-40}$. Complementary to A11 reactivity, AFM imaging of samples upon 1.5 h of incubation showed the presence of small oligomeric species for all Aβ peptides tested, including $A\beta_{1-38}$ and $A\beta_{1-40}$ (Fig. 2*B*). Even though oligomers were present for all Aβ peptides tested, $A\beta_{1-38}$ and $A\beta_{1-40}$ oligomers only developed into A11-positive oligomers at a later stage compared with $A\beta_{1-42}$ and $A\beta_{1-43}$. Cytotoxicity of oligomeric Aβ upon *C*-terminal variation was assessed using neuroblastoma cell line SH-SY5Y (Fig. 2*C*). A11-positive oligomers derived from $A\beta_{1-42}$ and $A\beta_{1-43}$ induced loss of cell viability at a concentration of 5 μM, whereas those derived of $A\beta_{1-38}$ and $A\beta_{1-40}$ affected cell viability only at a significantly higher concentration of 20 μM.

Aβ Lengths Display Conformational Differences—CD and FTIR spectroscopy were used to evaluate Aβ structure after 1.5 h of incubation. The spectra recorded for $A\beta_{1-38}$ and $A\beta_{1-40}$ using CD were very similar and displayed typical characteristics of a largely unstructured protein, whereas the spectra of $A\beta_{1-42}$ and $A\beta_{1-43}$ showed pronounced β-sheet formation with a minimum intensity at a wavelength of 218 nm (Fig. 3*A*). As FTIR is more sensitive to β-sheet formation than CD and can distinguish between parallel and anti-parallel β-sheet arrangements, FTIR measurements were performed complementary to CD. Fig. 3*B* shows difference spectra obtained by subtraction of the spectrum of non-aggregated Aβ (time 0) from the spectrum recorded after 1.5 h of incubation. The strong increase of absorbance at a wavelength of 1627 cm^{-1}, concurrent with a loss of signal between 1650–1655 cm^{-1} and 1680 cm^{-1} for all four peptides tested, indicated that β-sheet formation took place during the 1.5 h incubation time at the cost of random coil and β-turn structure. The more narrow peak for $A\beta_{1-38}$ suggests the formation of a more stable β-sheet as a result of more extensive H-bonding compared with the other peptide lengths investigated, although $A\beta_{1-40}$ was found to form most β-sheet judging from a higher signal intensity at a wavelength of 1627 cm^{-1}. The small increase at 1695 cm^{-1} seen here for $A\beta_{1-38}$ and $A\beta_{1-43}$ in addition to the increase at a wavelength of 1627 cm^{-1} reveals the formation of an antiparallel oriented β-sheet that has been typically used as a fingerprint for oligomer formation (42). Variation in evolution of these regions is observed between the Aβ isoforms. This observation suggests that the various Aβ isoforms display small structural differences during aggregation. Even though CD and FTIR provide useful structural information in terms of an average of the entire protein sequence, they do not provide insight into the behavior of individual residues in the sequence and, hence, are not able to address the question of why the addition of two valines in $A\beta_{1-40}$ rendered this peptide less aggregation-prone than $A\beta_{1-38}$. Also, CD and FTIR spectroscopy were unable to report on short-time scale conformational flexibility of peptides potentially required to trigger the onset of aggregation. We used MD simulations to establish whether individual residues contributed to changes in peptide conformation that

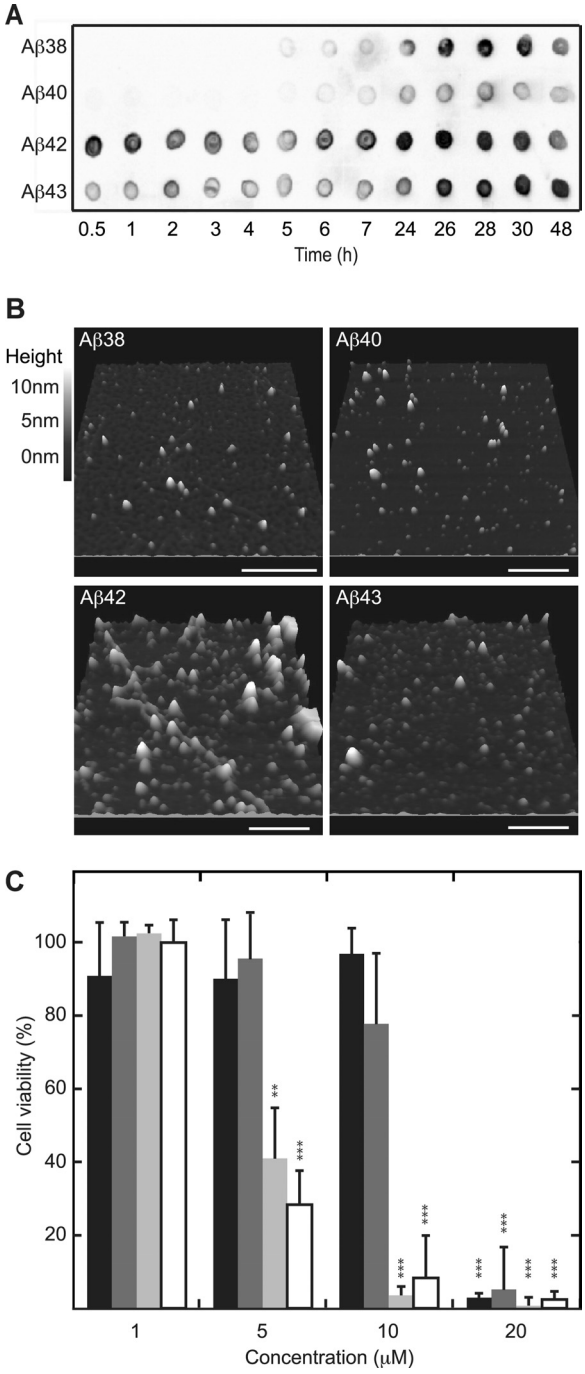

FIGURE 2. **Differences in aggregation kinetics due to C-terminal heterogeneity are reflected at toxic oligomer levels.** Aβ at 50 μM was allowed to aggregate at 25 °C under quiescent conditions. *A*, analysis with the A11 oligomer-specific antibody detected oligomeric $A\beta_{1-42}$ and $A\beta_{1-43}$ after as little as 0.5 h of incubation, whereas $A\beta_{1-38}$ and $A\beta_{1-40}$ became A11-positive after 5–6 h of incubation. *B*, imaging using AFM indicated the presence of oligomers for all Aβ samples incubated for 1.5 h. The *length of the bar* represents 500 nm. *C*, preincubated (1.5 h) Aβ was added to cultured SH-SY5Y cells and incubated for 24 h before probing cytotoxicity using Cell Titer Blue viability assay. $A\beta_{1-38}$ (*black*) and $A\beta_{1-40}$ (*dark gray*) only cause cytotoxicity at a concentration of 20 μM, whereas $A\beta_{1-42}$ (*light gray*) and $A\beta_{1-43}$ (*white*) are significantly cytotoxic at a concentration of 5 μM. Values are expressed as the percent of cell viability ± S.D. ($n = 4$), and buffer signal was normalized to 100%. Statistical significance (unpaired 2-tailed *t* test) compared with buffer control values (normalized to 100%) is indicated by *p* value analysis similar to Fig. 1*B*.

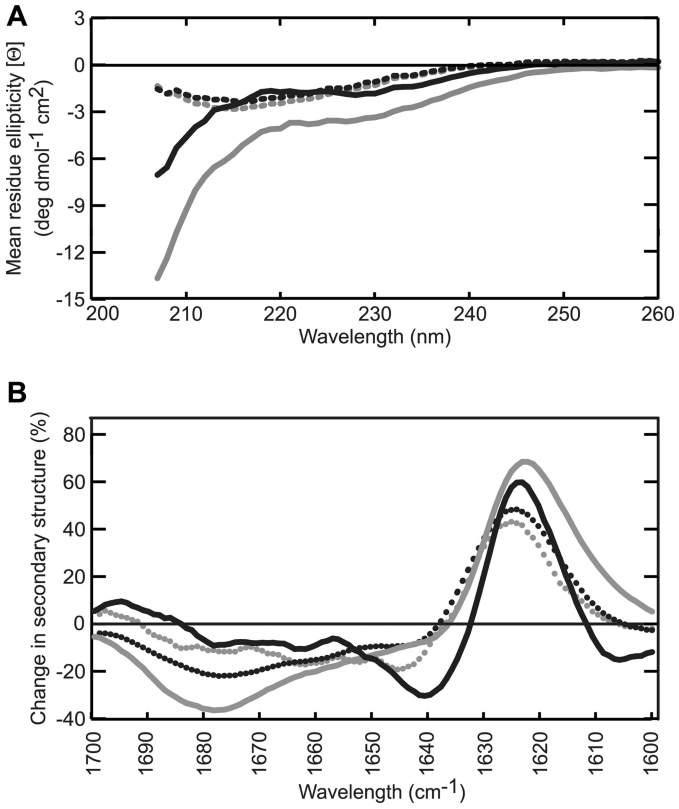

FIGURE 3. **Aggregating Aβ peptides show differences on a secondary structural level.** *A*, CD measurements were performed with preincubated (1.5 h) Aβ at 15 μM. Spectra recorded for $A\beta_{1-38}$ (*continuous black line*) and $A\beta_{1-40}$ (*continuous gray line*) were characteristic of peptides with a large degree of disorder, whereas $A\beta_{1-42}$ (*dotted black line*) and $A\beta_{1-43}$ (*dotted gray line*) displayed curves with a single minimum at 217 nm, suggesting β-sheet formation. High buffer interference was observed at wavelengths <207 nm. *B*, FTIR absorbance was measured of monomeric and preincubated (1.5 h) Aβ at 200 μM, and the difference between both spectra was plotted. The difference spectra showed an intensity increase at a wavelength of 1627 cm^{-1} indicating that all four peptides were converted into a β-sheet conformation. For $A\beta_{1-38}$ (*continuous black line*) and $A\beta_{1-43}$ (*dotted gray line*) an additional increase in intensity around 1695 cm^{-1} was observed implying an antiparallel oriented β-sheet. $A\beta_{1-40}$ (*continuous gray line*) and $A\beta_{1-42}$ (*dotted black line*) data were both characterized by a loss of β-turn as observed by the decrease in intensity at 1680 cm^{-1}.

could explain the observed results. We focused our observations on definition of secondary structure of proteins (DSSP) analysis (43). Here, we report the DSSP results as: coil (unstructured conformation), extended conformation (β-bridge plus β-sheet structures), loop (bend plus turns), and helical conformation (α-helix plus 3_{10}-helix plus π-helix). All peptides presented a general trend to possess a mixture of a collapsed coil structure and helical conformation for residues 1–20. N-terminal helical structure was partially retained over time, whereas C-terminal helicity, if any, was rapidly lost (supplemental Fig. 1). Also as a general observation, all extended conformations occurred between residues 21–28 and residues 32 to the C-terminal amino acid. A loop section comprising residues 29–31 formed flexible links between these extended portions. Contrary to what was expected, $A\beta_{1-38}$ conformation behavior most closely resembled that of $A\beta_{1-42}$ rather than $A\beta_{1-40}$ (Fig. 4, *A* and *B*, supplemental Fig. 1). Over the 100-ns time scale of the simulations, $A\beta_{1-38}$ showed a marked tendency to form extended conformations (Fig. 4, *A* and *B*), comparable with $A\beta_{1-42}$ and $A\beta_{1-43}$ (Fig. 4, *B* and *B1*). $A\beta_{1-40}$, on the other hand, exhibited low tendency to form extended conformations (Fig. 4*A*). Interestingly, during the first 10s of nanoseconds the behavior of $A\beta_{1-38}$ was erratic and fluctuated between resembling $A\beta_{1-40}$ and $A\beta_{1-42}$/$A\beta_{1-43}$. Only after 50 ns of simulation did the content of extended conformation invariably increase (Fig. 4, *A* and *D*). $A\beta_{1-42}$ and $A\beta_{1-43}$ seemed to accumulate and stabilize better than their extended conformations, from earlier simulation times onwards (Fig. 4, *B* and *B1*, supplemental Fig. 2). The same behavior was reflected in the overall helicity of the peptides (Fig. 4*C*) revealing a slight, yet statistically significant, higher tendency to retain its helical conformation for $A\beta_{1-38}$ in comparison to $A\beta_{1-42}$ and $A\beta_{1-43}$. A marked increase in the helicity of residues 20–23 and 28 was uniquely observed for $A\beta_{1-40}$ (Fig. 4, *C* and *D*). Collectively, these data showed that the behaviors of $A\beta_{1-42}$ and $A\beta_{1-43}$ were remarkably similar in terms of their high tendency to form an extended β-sheet conformation, whereas $A\beta_{1-40}$ retained helicity longer. The $A\beta_{1-38}$ peptide showed very interesting behavior in terms of its highly fluctuating tendency to form extended β-sheet conformation. Over time $A\beta_{1-38}$ conformation alternated rapidly between $A\beta_{1-42}$/$A\beta_{1-43}$-like conformation and $A\beta_{1-40}$-like conformation before forming a stable, extended β-sheet.

Mixtures of Aβ Show Complex Aggregation Behavior—To evaluate the influence of the observed differences between Aβ isoforms in a more biologically relevant setting, we mimicked the complex pool of various Aβ peptide lengths as observed *in vivo* by preparing Aβ peptide mixtures containing $A\beta_{1-40}$, $A\beta_{1-42}$ and $A\beta_{1-38}$, or $A\beta_{1-43}$. Increased levels of $A\beta_{1-38}$ in the cerebrospinal fluid of AD patients are reported (24) as well as an increased generation of this peptide due to presinilin-1 mutations (44). Some forms of familial AD display increased generation of $A\beta_{1-43}$ (44), a peptide length frequently present in amyloid plaques (18). $A\beta_{1-40}$ and $A\beta_{1-43}$ were shown to directly interact using electrospray ionization-MS (supplemental Fig. 4*C*), although these dimeric species only accumulated at a population of ~1% (supplemental Fig. 3*C*). Effective but low accumulation of mixed dimers was also observed upon mixing $A\beta_{1-38}$ and $A\beta_{1-42}$ (supplemental Figs. 3*B* and 4*B*). Mixed dimeric complex formation was further detected for $A\beta_{1-38}$·$A\beta_{1-40}$ and $A\beta_{1-42}$·$A\beta_{1-43}$ (supplemental Fig. 3 and 4). Along the lines of the earlier-identified processing pathways of APP toward the formation of either $A\beta_{1-40}$ and $A\beta_{1-38}$ with $A\beta_{1-43}$ and $A\beta_{1-42}$ as intermediates, respectively (10), we mapped dose-response curves of the presence of $A\beta_{1-43}$ and $A\beta_{1-38}$ on the aggregation kinetics of $A\beta_{1-40}$ and $A\beta_{1-42}$, respectively, using ThT fluorescence (Fig. 5). We reported earlier that $A\beta_{1-42}$·$A\beta_{1-40}$ mixtures behave differently according to their proportional presence (26). Titration of $A\beta_{1-40}$ with increasing concentrations of $A\beta_{1-43}$ substantially reduced the lag phase of aggregation to become similar to that of $A\beta_{1-43}$ alone, whereas final fluorescence intensities were not affected (Fig. 5, *A*, and *C*). These observations suggest that $A\beta_{1-43}$ dominantly influences the nucleation process of $A\beta_{1-40}$, whereas aggregate morphology or mass were presumably determined by $A\beta_{1-40}$ (Fig. 5*C*). Titration of $A\beta_{1-38}$ with $A\beta_{1-42}$ similarly led to a decreased nucleation rate but, in addition, gradually increased the elongation rate and final ThT fluorescence intensity (Fig. 5, *B* and *D*).

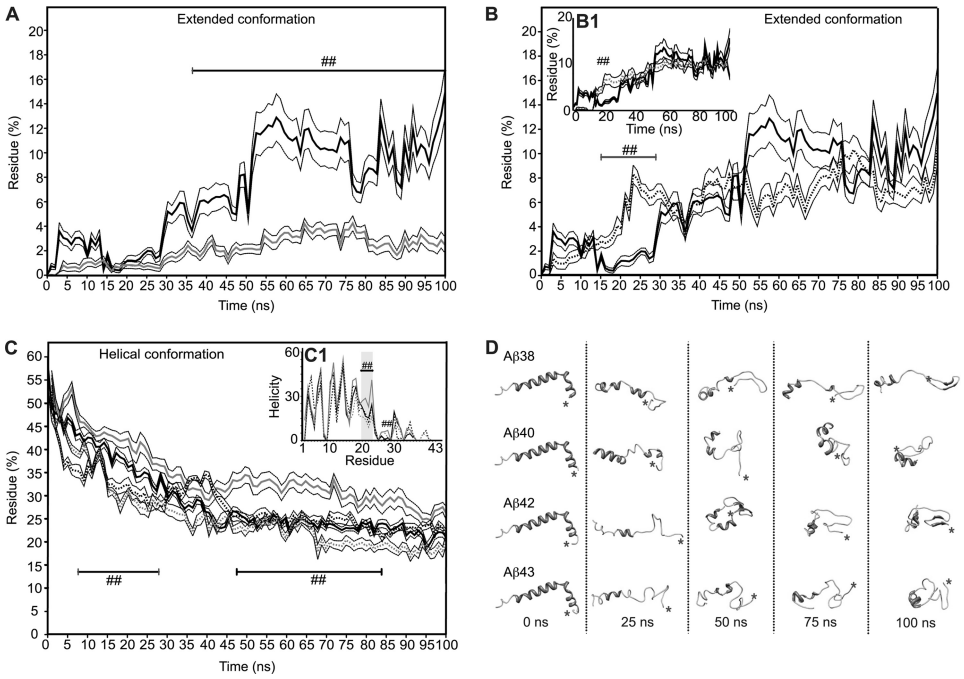

FIGURE 4. **Aβ peptides show conformational fluctuations at short time scales that vary upon C-terminal elongation.** Secondary structure composition was determined by the DSSP method: extended conformation (β-bridge plus β-sheet structures) and helical conformation (α-helix plus 3_{10}-helix plus π-helix). Results were averaged over 10 independent simulations. The extended conformation content in function of time for $A\beta_{1-38}$ (*continuous black line*) is compared with $A\beta_{1-40}$ (*continuous gray line*) (*A*) and $A\beta_{1-42}$ (*dotted black line*) (*B*); the inset plot (*B1*), $A\beta_{1-43}$ (*dotted gray line*), reveals a similar profile compared with $A\beta_{1-42}$. Statistically significant differences (S.E.) are denoted by ($p < 0.005$ (##)). *C*, the helical content in the function of time is shown for all peptides. Grayscale code is the same as for the previous panels. Regions of the simulation time wherein there are statistically significant differences are denoted by ($p < 0.005$ (##)) compared with $A\beta_{1-42}$. The inset (*C1*) shows helicity per residue for all Aβ peptides (##, $p < 0.005$, compared with all Aβ peptides). Helicity is reported as the percentage of simulation time that a given amino acid residue presented α-helix conformation. *D*, shown are snapshots for all Aβ peptides at 0, 25, 50, 75, and 100 ns of simulation time. C termini positions are denoted with an *asterisk* (*).

The complex aggregation characteristics compared with each of these peptides in isolation are highly suggestive of interaction of the Aβ peptides in mixtures.

$A\beta_{1-40}$ is the most predominant species recovered from cerebrospinal fluid (6, 45). $A\beta_{1-38}$ has been reported to be present in cerebrospinal fluid at concentrations of 1.26 to 2.78 ng/ml, whereas concentrations of $A\beta_{1-42}$ were 0.46 to 2.07 ng/ml (6, 45, 46). Quantitative detection of $A\beta_{1-43}$ has only been performed in brain plaques and, as suitable antibodies are not available, can generally not be distinguished from that of $A\beta_{1-42}$. Although quantitative information on the released amounts of the four Aβ isoforms of interest from APP is only available for FAD mutations based on *in vitro* observations (11, 44, 47, 48), we performed titration assays (Fig. 5). Results indicated that 30% of $A\beta_{1-38}$ or $A\beta_{1-43}$ already caused a significant alteration of the aggregation profile of $A\beta_{1-42}$ and of the lag phase of $A\beta_{1-40}$. Many FAD-related mutations accumulate $A\beta_{1-42}$, whereas it can be assumed that in sporadic AD $A\beta_{1-40}$ is predominantly produced (49). We, therefore, decided to evaluate the effect of small concentrations (10%) of $A\beta_{1-38}$ and $A\beta_{1-43}$ on predominantly present (90%) $A\beta_{1-40}$ and $A\beta_{1-42}$ to monitor more subtle influences of the presence of peptides in mixtures. In summary, we evaluated oligomerization, cytotoxicity, and aggregation of 9:1 mixtures of $A\beta_{1-40}$·$A\beta_{1-38}$, $A\beta_{1-40}$·$A\beta_{1-43}$, $A\beta_{1-42}$·$A\beta_{1-38}$, and $A\beta_{1-42}$·$A\beta_{1-43}$. At these low concentrations the effect of the addition of $A\beta_{1-38}$ and $A\beta_{1-43}$ to either $A\beta_{1-40}$ or $A\beta_{1-42}$ was limited to a significant decrease in final fluorescence intensity while leaving the nucleation phase unchanged (Fig. 6, *A* and *B*). Visualization of aggregate morphology by transmission electron microscopy further rationalized the observed change in final fluorescence intensity (Figs. 1*C* and 6*C*). Even though aggregate formation could not be established at early time points for $A\beta_{1-38}$ and $A\beta_{1-40}$ in isolation, a 9:1 mixture of these peptides showed the formation of extensive ThT-negative but A11-positive aggregates that were present for extended periods of time (Fig. 6, *A*, *C*, and *D*). Also, at early time points of incubation the morphologies of both $A\beta_{1-40}$ and $A\beta_{1-42}$ in mixtures (Fig. 6*C*) appear different from these peptides in isolation (compare with Fig. 1*C*). Upon extended incubation, all mixtures aggregated into morphologically similar networks of long, interacting fibrils, similar to those observed for peptides in isolation (Fig. 6*C*). The observed differences in A11 interaction and aggregate morphology further led us to investigate the cytotoxic response of Aβ mixtures using cultured SH-SY5Y cells. Interestingly, even though $A\beta_{1-38}$ or $A\beta_{1-40}$ in isolation induced no cytotoxic response below a concentration of 20 μM, the addition of $A\beta_{1-38}$ to $A\beta_{1-40}$ resulted in a pronounced and significant loss of cell viability at a total peptide concentration of 10 μM, consistent with the A11-positive response for this mixture (Fig. 6, *D* and *E*). Strikingly, the addition of $A\beta_{1-38}$ to $A\beta_{1-42}$ instead exerted a cytoprotective effect despite showing the formation of A11-positive oligomers, preventing loss of cell viability up to a total Aβ concentration of 10 μM. In addition to this, even though both $A\beta_{1-42}$ and $A\beta_{1-43}$ are similarly cytotoxic at a concentration of 10 μM, the mixture of these two peptides alleviates the

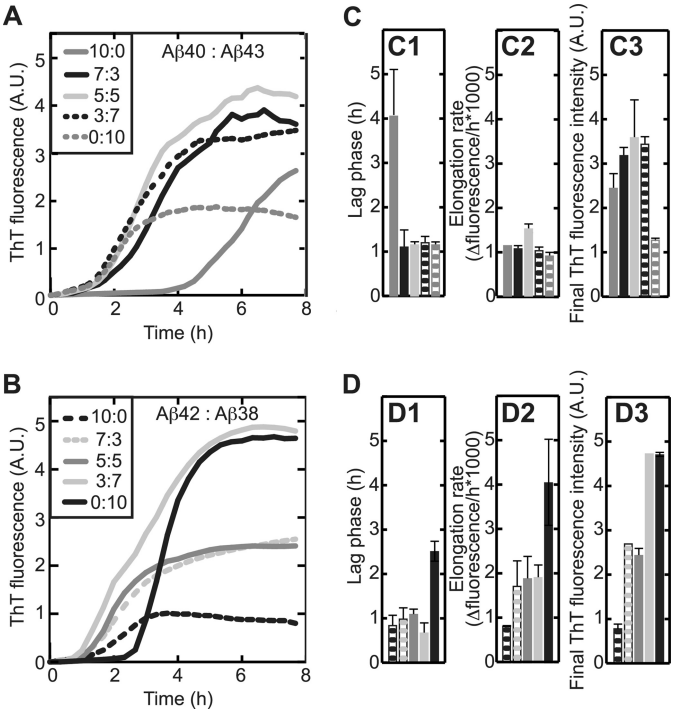

FIGURE 5. **Little prevalent Aβ peptides strongly affect the behavior of predominant Aβ.** ThT fluorescence was recorded *in situ* every 5 min at 25 °C with 50 μM Aβ and 12 μM ThT. Values represent the means of two experiments. *A* and *C*, irrespective of its concentration, $A\beta_{1-43}$ (*dotted gray line*) reduced the lag phase for aggregation (*C1*) of $A\beta_{1-40}$ (*continuous gray line*) without affecting elongation rates (*C2*). $A\beta_{1-40}$·$A\beta_{1-43}$ mixtures displayed higher fluorescence intensity after 8 h incubation (*C3*) than $A\beta_{1-40}$ and $A\beta_{1-43}$ alone. Grayscale code is as in *A*. *B* and *D*, titration of $A\beta_{1-42}$ (*dotted black line*) with $A\beta_{1-38}$ (*continuous black line*) reduced lag phase (*D1*) and elongation rate (*D2*) but increased fluorescence intensity at plateau (*D3*). Grayscale code is as in Fig. *B*. *A.U.*, absorbance units.

cytotoxic response, whereas $A\beta_{1-43}$ induces cytotoxicity in the presence of $A\beta_{1-40}$.

Collectively, our data suggest that, apart from distinct propensities to form cytotoxic oligomers and aggregates for individual Aβ peptides, mixtures of various Aβ peptides do not behave in a predictable manner according to a simple additive effect but can actively modulate the behavior of other isoforms present in the mixture to either induce or prevent toxicity or modify their aggregation propensities.

DISCUSSION

Aβ aggregation is a complex process during which a monomeric population progressively self-assembles first into oligomers and finally into mature fibrils. We show that biologically relevant mixtures of Aβ peptides containing $A\beta_{1-38}$, $A\beta_{1-40}$, $A\beta_{1-42}$, and $A\beta_{1-43}$ behave in a more complex manner than can be anticipated from their behaviors in isolation with direct consequences for their oligomerization, aggregation, and cytotoxic behavior. We also report that co-occurring Aβ peptides can affect each other by conformational modulation of the C-terminal region that, in turn, is a function of C-terminal flexibility to adopt various conformations. For example, $A\beta_{1-38}$ in isolation exhibited little cytotoxic potential, similar to $A\beta_{1-40}$. At the same time, cytotoxic oligomers accumulated rapidly for $A\beta_{1-42}$ and $A\beta_{1-43}$. Nevertheless, mixtures of $A\beta_{1-38}$ and $A\beta_{1-40}$ were highly toxic, whereas the addition of $A\beta_{1-38}$ to $A\beta_{1-42}$ surprisingly induced a cytoprotective effect. The A11 reactivity of the individual Aβ peptides in isolation correlated with the observed cytotoxicity, although all isoforms were found to form oligomers. This observation suggests a conformational difference between oligomers of different isoforms. The presence of both toxic A11-positive and non-toxic A11-negative oligomers has been reported recently for Aβ as well as for the yeast-sup35 protein (50, 51). The cytotoxicity-A11 reactivity correlation for peptides in isolation could not be extended to mixtures of Aβ isoforms. This lack of correlation can be explained by the polyclonal nature of the antibody to recognize non-toxic oligomers in addition to toxic species. Another possibility is that non-toxic and toxic oligomers are both formed and that the variation in signal intensities and cytotoxicity arises from the variation in the distribution between these oligomers. At high concentrations when the level of toxic oligomers is sufficiently high, the shorter Aβ isoforms become similar cytotoxic to the longer Aβ isoforms. Although not being able to reveal distinct accumulation of specific conformations using CD, FTIR revealed small structural differences during a 1.5-h incubation time. Even though all tested Aβ peptides showed substantial β-sheet formation over time, only for $A\beta_{1-38}$ and $A\beta_{1-43}$ anti-parallel β-sheet formation could be identified that has been interpreted previously as typical for oligomer formation (42). As both FTIR and CD are only informative on an ensemble level, we used MD to elucidate the short-time scale dynamic behavior of the peptides. MD simulations revealed that both $A\beta_{1-38}$ and $A\beta_{1-42}$ gained extended β-sheet conformation rapidly, whereas helicity in $A\beta_{1-40}$ was retained for longer, which is in good agreement with earlier reports (52). In line with our findings, it has previously been reported that stabilization of the central α-helical region of Aβ by ligands or mutations results in a significant delay of aggregation (53–55) and that inhibition of unfolding of the central α-helical region increases longevity in a *Drosophila* model of AD (54). At the same time, rapid induction of extended β-sheet formation has been found to have a strong predictive power in terms of toxic potential rationalizing the development of so-called β-sheet breakers as a therapeutic approach (for review, see Ref. 56). Interestingly, $A\beta_{1-38}$ showed behavior that could be explained by rapid gain and loss of extended β-sheet conformation, fluctuating in behavior between $A\beta_{1-40}$ and $A\beta_{1-42}$/$A\beta_{1-43}$, respectively. Rapid conformational switching between distinct conformations has been observed before for synaptically confined proteins SNAP-25 and synaptobrevin and was proposed to characterize a specific class of intrinsically disordered proteins (57). Conformational flexibility was suggested to allow for fast ligand interaction and conformational selection, which potentially has functional implications for the findings we report on $A\beta_{1-38}$ but which warrant further investigation. The presence of other peptides with higher preference of one over another conformation may drive $A\beta_{1-38}$ to rapidly recognize these as a potential ligand and template for conformational selection, which in turn either induces or inhibits aggregation. However, this may be an oversimplification of the actual situation as $A\beta_{1-42}$ in the presence of $A\beta_{1-38}$ is in fact less toxic, which does not comply with this suggestion. Further research is required to precisely underpin the molecular mechanism of this

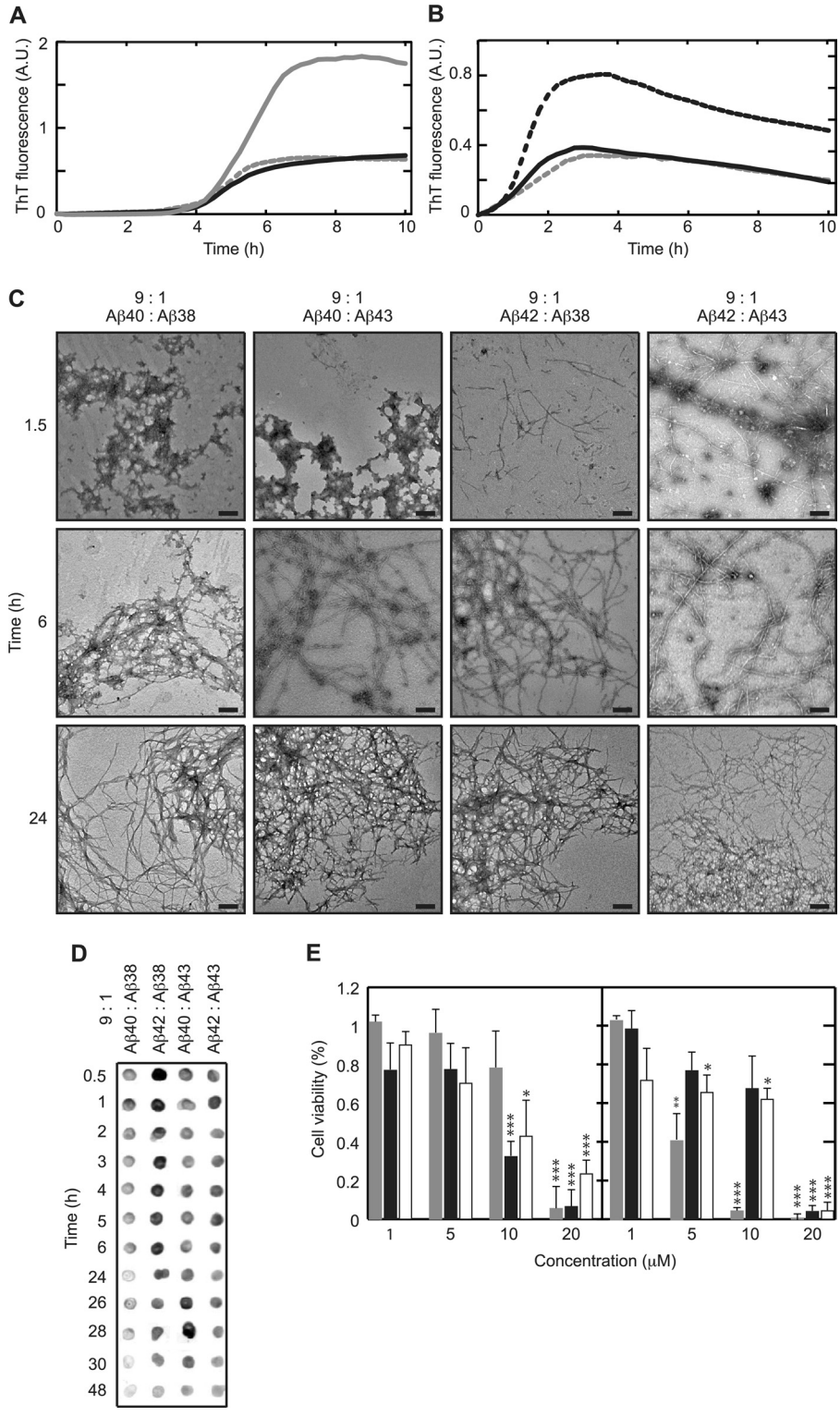

FIGURE 6. **Aβ peptides in mixtures display complex aggregation behavior and toxicity.** *A* and *B*, the addition of 10% (=5 μM) $A\beta_{1-38}$ (*continuous black line*) or $A\beta_{1-43}$ (*dotted gray line*) to 90% (=45 μM) $A\beta_{1-40}$ (*continuous gray line*) or $A\beta_{1-42}$ (*dotted black line*) decreased the final (10 h) ThT fluorescence compared with $A\beta_{1-40}$ or $A\beta_{1-42}$ alone. Values represent the means of three experiments (*C*). After 1.5 h of incubation, mixtures containing $A\beta_{1-38}$ formed amorphous aggregates, whereas mixtures containing $A\beta_{1-43}$ formed short fibrillar structures. Longer incubation for 6 h resulted in fibrillar networks for all mixtures, which extended into dense, highly intertwined, stained networks after 24 h of incubation. The length of the *scale bar* is 200 nm. *D*, all Aβ mixtures intensively reacted with A11 oligomer-specific antibody after 0.5 h of incubation, which gradually decreased upon longer incubation dependent on the Aβ mixture. *E*, Aβ was added to cultured SH-SY5Y cells and incubated for 24 h before probing cytotoxicity using the Cell Titer Blue viability assay. Note that non-toxic $A\beta_{1-40}$ (*left*, *gray*) became highly toxic upon mixing with non-toxic $A\beta_{1-38}$ (*left*, *black*) and $A\beta_{1-43}$ (*left*, *white*) at a concentration of 10 μM. Toxicity of $A\beta_{1-42}$ (*right*, *gray*) is reduced upon the addition of $A\beta_{1-38}$ (*right*, *black*) or $A\beta_{1-43}$ (*right*, *white*). Values are the percent of cell viability ± S.D. ($n = 4$), and buffer signal was normalized to 100%. Statistical significance (unpaired 2-tailed *t* test) compared with buffer control is indicated by *** ($p < 0.0001$), ** ($p < 0.0005$), and * ($p < 0.005$). *A.U.*, absorbance units.

observation. It has been previously reported that Glu^{22}, Asp^{23}, and Lys^{28} play a critical role in the aggregation process (58–61). Presumably, Asp^{23} (and Lys^{28}), although residing in a helical conformation, may not be able to trigger the formation of extended conformations, at least at early time points, thus retarding the aggregation of $A\beta_{1-40}$. Therefore, not only the unfolding rate of the C-terminus, as has been previously suggested, can dictate the potential event to trigger aggregation and toxicity of Aβ (60), but also the capability of a given Aβ peptide to retain its helical conformation may be considered to induce such events. Based on the outcome of our MD simulations, we suggest that the plastic behavior of $A\beta_{1-38}$, inducing toxicity for $A\beta_{1-40}$ while eliminating response to $A\beta_{1-42}$, plays a key role to these observations. Hence, the presence of other peptides may direct the self-assembly process toward at least two possible pathways, one leading to toxic oligomers and the second leading to non-toxic intermediates. $A\beta_{1-43}$ does not display fluctuating secondary structures and rapidly forms extended β-sheets. The self-assembly process in the presence of other peptides is, therefore, probably more dependent on the flexibility of the structure of the second peptide. Indeed, it has been shown for the N-terminal domain of the HypF protein from *Escherichia coli* that both toxic and non-toxic oligomers can be formed (62).

Overall, our results can be of major importance for the further development of therapeutic strategies. The current approach of modulating γ-secretase activity to decrease $A\beta_{1-42}$ generation results in increased $A\beta_{1-38}$ levels at the same time. This approach is based on the observation that longer Aβ isoforms are more aggregation-prone. Hence, establishing an increased $A\beta_{1-38}$ level is considered a suitable and non-toxic approach to inhibit AD disease progress without compromising the important multi-substrate processing by γ-secretase. However, clinical studies still have to confirm their disease-modulating capacity. Whether this is due to the low brain-barrier penetrating potency of the compounds being tested requires further investigation. Together with previously published data (44), our results possibly indicate that another explanation for the lack of clinical evidence to place GSMs firmly on the map as AD therapy may be the induction of adverse, unexpected events as a result of the increased $A\beta_{1-38}$ levels in combination with other Aβ peptides. In this view, Golde *et al.* (63) recently argued that the efficiency of different GSMs to shift Aβ release toward shorter isoforms could determine their therapeutic potential. We propose that peptide conformational flexibility may confer toxic properties to its oligomers and underline the importance of understanding the interplay between various Aβ isoforms.

Acknowledgments—We thank Maja Debulpaep for instructions and technical assistance with transmission electron microscopy and Kim Sweers and Ine Segers-Nolten for support during AFM measurements.

REFERENCES

1. Glenner, G. G., and Wong, C. W. (1984) Alzheimer disease. Initial report of the purification and characterization of a novel cerebrovascular amyloid protein. *Biochem. Biophys. Res. Commun.* **120,** 885–890
2. Haass, C., Schlossmacher, M. G., Hung, A. Y., Vigo-Pelfrey, C., Mellon, A., Ostaszewski, B. L., Lieberburg, I., Koo, E. H., Schenk, D., and Teplow, D. B. (1992) Amyloid β-peptide is produced by cultured cells during normal metabolism. *Nature* **359,** 322–325
3. De Strooper, B., Saftig, P., Craessaerts, K., Vanderstichele, H., Guhde, G., Annaert, W., Von Figura, K., and Van Leuven, F. (1998) Deficiency of presenilin-1 inhibits the normal cleavage of amyloid precursor protein. *Nature* **391,** 387–390
4. Yan, R., Bienkowski, M. J., Shuck, M. E., Miao, H., Tory, M. C., Pauley, A. M., Brashier, J. R., Stratman, N. C., Mathews, W. R., Buhl, A. E., Carter, D. B., Tomasselli, A. G., Parodi, L. A., Heinrikson, R. L., and Gurney, M. E. (1999) Membrane-anchored aspartyl protease with Alzheimer disease β-secretase activity. *Nature* **402,** 533–537
5. Vigo-Pelfrey, C., Lee, D., Keim, P., Lieberburg, I., and Schenk, D. B. (1993) Characterization of β-amyloid peptide from human cerebrospinal fluid. *J. Neurochem.* **61,** 1965–1968
6. Wiltfang, J., Esselmann, H., Bibl, M., Smirnov, A., Otto, M., Paul, S., Schmidt, B., Klafki, H. W., Maler, M., Dyrks, T., Bienert, M., Beyermann, M., Rüther, E., and Kornhuber, J. (2002) Highly conserved and disease-specific patterns of carboxyl-terminal-truncated Aβ peptides 1–37/38/39 in addition to 1–40/42 in Alzheimer disease and in patients with chronic neuroinflammation. *J. Neurochem.* **81,** 481–496
7. Gu, Y., Misonou, H., Sato, T., Dohmae, N., Takio, K., and Ihara, Y. (2001) Distinct intramembrane cleavage of the β-amyloid precursor protein family resembling γ-secretase-like cleavage of Notch. *J. Biol. Chem.* **276,** 35235–35238
8. Sato, T., Dohmae, N., Qi, Y., Kakuda, N., Misonou, H., Mitsumori, R., Maruyama, H., Koo, E. H., Haass, C., Takio, K., Morishima-Kawashima, M., Ishiura, S., and Ihara, Y. (2003) Potential link between amyloid β-protein 42 and C-terminal fragment γ49–99 of β-amyloid precursor protein. *J. Biol. Chem.* **278,** 24294–24301
9. Qi-Takahara, Y., Morishima-Kawashima, M., Tanimura, Y., Dolios, G., Hirotani, N., Horikoshi, Y., Kametani, F., Maeda, M., Saido, T. C., Wang, R., and Ihara, Y. (2005) Longer forms of amyloid β protein. Implications for the mechanism of intramembrane cleavage by γ-secretase. *J. Neurosci.* **25,** 436–445
10. Takami, M., Nagashima, Y., Sano, Y., Ishihara, S., Morishima-Kawashima, M., Funamoto, S., and Ihara, Y. (2009) γ-Secretase. Successive tripeptide and tetrapeptide release from the transmembrane domain of β-carboxyl terminal fragment. *J. Neurosci.* **29,** 13042–13052
11. Bentahir, M., Nyabi, O., Verhamme, J., Tolia, A., Horré, K., Wiltfang, J., Esselmann, H., and De Strooper, B. (2006) Presenilin clinical mutations can affect γ-secretase activity by different mechanisms. *J. Neurochem.* **96,** 732–742
12. Saito, T., Suemoto, T., Brouwers, N., Sleegers, K., Funamoto, S., Mihira, N., Matsuba, Y., Yamada, K., Nilsson, P., Takano, J., Nishimura, M., Iwata, N., Van Broeckhoven, C., Ihara, Y., and Saido, T. C. (2011) Potent amyloidogenicity and pathogenicity of Aβ43. *Nat. Neurosci.* **14,** 1023–1032
13. Jarrett, J. T., and Lansbury, P. T. (1993) Seeding "one-dimensional crystallization" of amyloid. A pathogenic mechanism in Alzheimer disease and scrapie? *Cell* **73,** 1055–1058
14. Bitan, G., Kirkitadze, M. D., Lomakin, A., Vollers, S. S., Benedek, G. B., and Teplow, D. B. (2003) Amyloid β-protein (Aβ) assembly. Aβ40 and Aβ42 oligomerize through distinct pathways. *Proc. Natl. Acad. Sci. U.S.A.* **100,** 330–335
15. Benseny-Cases, N., Cócera, M., and Cladera, J. (2007) Conversion of non-fibrillar β-sheet oligomers into amyloid fibrils in Alzheimer disease amyloid peptide aggregation. *Biochem. Biophys. Res. Commun.* **361,** 916–921
16. Gravina, S. A., Ho, L., Eckman, C. B., Long, K. E., Otvos, L., Jr., Younkin, L. H., Suzuki, N., and Younkin, S. G. (1995) Amyloid β protein (Aβ) in Alzheimer disease brain. Biochemical and immunocytochemical analysis with antibodies specific for forms ending at Aβ 40 or Aβ42(43). *J. Biol. Chem.* **270,** 7013–7016
17. Iwatsubo, T., Saido, T. C., Mann, D. M., Lee, V. M., and Trojanowski, J. Q. (1996) Full-length amyloid-β(1–42 (43)) and amino-terminally modified and truncated amyloid-β42 (43) deposit in diffuse plaques. *Am. J. Pathol.* **149,** 1823–1830
18. Welander, H., Frånberg, J., Graff, C., Sundström, E., Winblad, B., and Tjernberg, L. O. (2009) Aβ43 is more frequent than Aβ40 in amyloid

plaque cores from Alzheimer disease brains. *J. Neurochem.* **110,** 697–706
19. Weggen, S., Eriksen, J. L., Das, P., Sagi, S. A., Wang, R., Pietrzik, C. U., Findlay, K. A., Smith, T. E., Murphy, M. P., Bulter, T., Kang, D. E., Marquez-Sterling, N., Golde, T. E., and Koo, E. H. (2001) A subset of NSAIDs lower amyloidogenic Aβ42 independently of cyclooxygenase activity. *Nature* **414,** 212–216
20. Eriksen, J. L., Sagi, S. A., Smith, T. E., Weggen, S., Das, P., McLendon, D. C., Ozols, V. V., Jessing, K. W., Zavitz, K. H., Koo, E. H., and Golde, T. E. (2003) NSAIDs and enantiomers of flurbiprofen target γ-secretase and lower Aβ42 *in vivo*. *J. Clin. Invest.* **112,** 440–449
21. Laino, C. (2009) In follow-up analysis of clinical trial, NSAIDs seem to preserve cognitive function in patients with healthy brains. *Neurol. Today* **9,** 21–22
22. Oehlrich, D., Berthelot, D. J., and Gijsen, H. J. (2011) γ-Secretase modulators as potential disease modifying anti-Alzheimer drugs. *J. Med. Chem.* **54,** 669–698
23. Imbimbo, B. P., and Giardina, G. A. (2011) γ-Secretase inhibitors and modulators for the treatment of Alzheimer disease. Disappointments and hopes. *Curr. Top. Med. Chem.* **11,** 1555–1570
24. Lewczuk, P., Esselmann, H., Meyer, M., Wollscheid, V., Neumann, M., Otto, M., Maler, J. M., Rüther, E., Kornhuber, J., and Wiltfang, J. (2003) The amyloid-β (Aβ) peptide pattern in cerebrospinal fluid in Alzheimer disease. Evidence of a novel carboxyl-terminal-elongated Aβ peptide. *Rapid Commun. Mass Spectrom.* **17,** 1291–1296
25. Maddalena, A. S., Papassotiropoulos, A., Gonzalez-Agosti, C., Signorell, A., Hegi, T., Pasch, T., Nitsch, R. M., and Hock, C. (2004) Cerebrospinal fluid profile of amyloid β peptides in patients with Alzheimer disease determined by protein biochip technology. *Neurodegener. Dis.* **1,** 231–235
26. Kuperstein, I., Broersen, K., Benilova, I., Rozenski, J., Jonckheere, W., Debulpaep, M., Vandersteen, A., Segers-Nolten, I., Van Der Werf, K., Subramaniam, V., Braeken, D., Callewaert, G., Bartic, C., D'Hooge, R., Martins, I. C., Rousseau, F., Schymkowitz, J., and De Strooper, B. (2010) Neurotoxicity of Alzheimer disease Aβ peptides is induced by small changes in the $Aβ_{42}$ to $Aβ_{40}$ ratio. *EMBO J.* **29,** 3408–3420
27. Broersen, K., Jonckheere, W., Rozenski, J., Vandersteen, A., Pauwels, K., Pastore, A., Rousseau, F., and Schymkowitz, J. (2011) A standardized and biocompatible preparation of aggregate-free amyloid β peptide for biophysical and biological studies of Alzheimer disease. *Protein Eng. Des. Sel.* **24,** 743–750
28. Kayed, R., Head, E., Thompson, J. L., McIntire, T. M., Milton, S. C., Cotman, C. W., and Glabe, C. G. (2003) Common structure of soluble amyloid oligomers implies common mechanism of pathogenesis. *Science* **300,** 486–489
29. Fernandez-Escamilla, A. M., Rousseau, F., Schymkowitz, J., and Serrano, L. (2004) Prediction of sequence-dependent and mutational effects on the aggregation of peptides and proteins. *Nat. Biotechnol.* **22,** 1302–1306
30. Kang, J., Lemaire, H. G., Unterbeck, A., Salbaum, J. M., Masters, C. L., Grzeschik, K. H., Multhaup, G., Beyreuther, K., and Müller-Hill, B. (1987) The precursor of Alzheimer disease amyloid A4 protein resembles a cell-surface receptor. *Nature* **325,** 733–736
31. Jorgensen, W. L., and Tirado-Rives, J. (1988) The OPLS potential functions for proteins, energy minimizations for crystals of cyclic peptides and crambin. *J. Am. Chem. Soc.* **110,** 1657–1666
32. Hess, B., Bekker, H., Berendsen, H. J. C., and Fraaije, J. G. E. M. (1997) LINCS. A linear constraint solver for molecular simulations. *J. Comput. Chem.* **18,** 1463–1472
33. Pettersen, E. F., Goddard, T. D., Huang, C. C., Couch, G. S., Greenblatt, D. M., Meng, E. C., and Ferrin, T. E. (2004) UCSF Chimera. A visualization system for exploratory research and analysis. *J. Comput. Chem.* **25,** 1605–1612
34. Harper, J. D., and Lansbury, P. T. (1997) Models of amyloid seeding in Alzheimer disease and scrapie. Mechanistic truths and physiological consequences of the time-dependent solubility of amyloid proteins. *Annu. Rev. Biochem.* **66,** 385–407
35. Biancalana, M., and Koide, S. (2010) Molecular mechanism of thioflavin-T binding to amyloid fibrils. *Biochim. Biophys. Acta* **1804,** 1405–1412
36. Stine, W. B., Jr., Snyder, S. W., Ladror, U. S., Wade, W. S., Miller, M. F., Perun, T. J., Holzman, T. F., and Krafft, G. A. (1996) The nanometer-scale structure of amyloid-β visualized by atomic force microscopy. *J. Protein Chem.* **15,** 193–203
37. Röhrig, U. F., Laio, A., Tantalo, N., Parrinello, M., and Petronzio, R. (2006) Stability and structure of oligomers of the Alzheimer β peptide $Aβ_{16-22}$. From the dimer to the 32-mer. *Biophys. J.* **91,** 3217–3229
38. LeVine, H., 3rd (1993) Thioflavine T interaction with synthetic Alzheimer disease β-amyloid peptides. Detection of amyloid aggregation in solution. *Protein Sci.* **2,** 404–410
39. Lambert, M. P., Barlow, A. K., Chromy, B. A., Edwards, C., Freed, R., Liosatos, M., Morgan, T. E., Rozovsky, I., Trommer, B., Viola, K. L., Wals, P., Zhang, C., Finch, C. E., Krafft, G. A., and Klein, W. L. (1998) Diffusible, nonfibrillar ligands derived from $Aβ_{1-42}$ are potent central nervous system neurotoxins. *Proc. Natl. Acad. Sci. U.S.A.* **95,** 6448–6453
40. Lesné, S., Koh, M. T., Kotilinek, L., Kayed, R., Glabe, C. G., Yang, A., Gallagher, M., and Ashe, K. H. (2006) A specific amyloid-β protein assembly in the brain impairs memory. *Nature* **440,** 352–357
41. Ahmed, M., Davis, J., Aucoin, D., Sato, T., Ahuja, S., Aimoto, S., Elliott, J. I., Van Nostrand, W. E., and Smith, S. O. (2010) Structural conversion of neurotoxic amyloid-$β_{1-42}$ oligomers to fibrils. *Nat. Struct. Mol. Biol.* **17,** 561–567
42. Cerf, E., Sarroukh, R., Tamamizu-Kato, S., Breydo, L., Derclaye, S., Dufrêne, Y. F., Narayanaswami, V., Goormaghtigh, E., Ruysschaert, J. M., and Raussens, V. (2009) Antiparallel β-sheet. A signature structure of the oligomeric amyloid β-peptide. *Biochem. J.* **421,** 415–423
43. Kabsch, W., and Sander, C. (1983) Dictionary of protein secondary structure. Pattern recognition of hydrogen-bonded and geometrical features. *Biopolymers* **22,** 2577–2637
44. Chávez-Gutiérrez, L., Bammens, L., Benilova, I., Vandersteen, A., Benurwar, M., Borgers, M., Lismont, S., Zhou, L., Van Cleynenbreugel, S., Esselmann, H., Wiltfang, J., Serneels, L., Karran, E., Gijsen, H., Schymkowitz, J., Rousseau, F., Broersen, K., and De Strooper, B. (2012) The mechanism of γ-secretase dysfunction in familial Alzheimer disease. *EMBO J.* **31,** 2261–2274
45. Bibl, M., Mollenhauer, B., Wolf, S., Esselmann, H., Lewczuk, P., Kornhuber, J., and Wiltfang, J. (2007) Reduced CSF carboxyl-terminal-truncated Aβ peptides in frontotemporal lobe degenerations. *J. Neural. Transm.* **114,** 621–628
46. Mann, D. M., Iwatsubo, T., Ihara, Y., Cairns, N. J., Lantos, P. L., Bogdanovic, N., Lannfelt, L., Winblad, B., Maat-Schieman, M. L., and Rossor, M. N. (1996) Predominant deposition of amyloid-β42(43) in plaques in cases of Alzheimer disease and hereditary cerebral hemorrhage associated with mutations in the amyloid precursor protein gene. *Am. J. Pathol.* **148,** 1257–1266
47. Scheuner, D., Eckman, C., Jensen, M., Song, X., Citron, M., Suzuki, N., Bird, T. D., Hardy, J., Hutton, M., Kukull, W., Larson, E., Levy-Lahad, E., Viitanen, M., Peskind, E., Poorkaj, P., Schellenberg, G., Tanzi, R., Wasco, W., Lannfelt, L., Selkoe, D., and Younkin, S. (1996) Secreted amyloid β-protein similar to that in the senile plaques of Alzheimer disease is increased *in vivo* by the presenilin 1 and 2 and APP mutations linked to familial Alzheimer disease. *Nature Med.* **2,** 864–870
48. Citron, M., Westaway, D., Xia, W., Carlson, G., Diehl, T., Levesque, G., Johnson-Wood, K., Lee, M., Seubert, P., Davis, A., Kholodenko, D., Motter, R., Sherrington, R., Perry, B., Yao, H., Strome, R., Lieberburg, I., Rommens, J., Kim, S., Schenk, D., Fraser, P., St George Hyslop, P., and Selkoe, D. J. (1997) Mutant presenilins of Alzheimer disease increase production of 42-residue amyloid β-protein in both transfected and transgenic mice. *Nature Med.* **3,** 67–72
49. Younkin, S. G. (1998) The role of Aβ42 in Alzheimer disease. *J. Physiol. Paris* **92,** 289–292
50. Krishnan, R., Goodman, J. L., Mukhopadhyay, S., Pacheco, C. D., Lemke, E. A., Deniz, A. A., and Lindquist, S. (2012) Conserved features of intermediates in amyloid assembly determine their benign or toxic states. *Proc. Natl. Acad. Sci. U.S.A.* **109,** 11172–11177
51. Ladiwala, A. R., Litt, J., Kane, R. S., Aucoin, D. S., Smith, S. O., Ranjan, S., Davis, J., Van Nostrand, W. E., and Tessier, P. M. (2012) Conformational differences between two amyloid β oligomers of similar size and dissimilar toxicity. *J. Biol. Chem.* **287,** 24765–24773
52. Shen, L., Ji, H. F., and Zhang, H. Y. (2008) Why is the C-terminus of Aβ(1–42) more unfolded than that of Aβ(1–40)? Clues from hydropho-

bic interaction. *J. Phys. Chem. B.* **112,** 3164–3167
53. Päiviö, A., Nordling, E., Kallberg, Y., Thyberg, J., and Johansson, J. (2004) Stabilization of discordant helices in amyloid fibril-forming proteins. *Protein Sci.* **13,** 1251–1259
54. Nerelius, C., Sandegren, A., Sargsyan, H., Raunak, R., Leijonmarck, H., Chatterjee, U., Fisahn, A., Imarisio, S., Lomas, D. A., Crowther, D. C., Strömberg, R., and Johansson, J. (2009) α-Helix targeting reduces amyloid-β peptide toxicity. *Proc. Natl. Acad. Sci. U.S.A.* **106,** 9191–9196
55. Ito, M., Johansson, J., Strömberg, R., and Nilsson, L. (2011) Unfolding of the amyloid β-peptide central helix. Mechanistic insights from molecular dynamics simulations. *PLoS ONE* **6,** e17587
56. Wisniewski, T., and Sadowski, M. (2008) *BMC Neurosci.* **9,** S5
57. Choi, U. B., McCann, J. J., Weninger, K. R., and Bowen, M. E. (2011) Beyond the random coil. Stochastic conformational switching in intrinsically disordered proteins. *Structure* **19,** 566–576
58. Borreguero, J. M., Urbanc, B., Lazo, N. D., Buldyrev, S. V., Teplow, D. B., and Stanley, H. E. (2005) Folding events in the 21–30 region of amyloid β-protein (Aβ) studied in silico. *Proc. Natl. Acad. Sci. U.S.A.* **102,** 6015–6020
59. Lazo, N. D., Grant, M. A., Condron, M. C., Rigby, A. C., and Teplow, D. B. (2005) On the nucleation of amyloid β-protein monomer folding. *Protein Sci.* **14,** 1581–1596
60. Baumketner, A., Bernstein, S. L., Wyttenbach, T., Lazo, N. D., Teplow, D. B., Bowers, M. T., and Shea, J. E. (2006) Structure of the 21–30 fragment of amyloid β-protein. *Protein Sci.* **15,** 1239–1247
61. Masman, M. F., Eisel, U. L., Csizmadia, I. G., Penke, B., Enriz, R. D., Marrink, S. J., and Luiten, P. G. (2009) *In silico* study of full-length amyloid β 1–42 tri- and penta-oligomers in solution. *J. Phys. Chem. B.* **113,** 11710–11719
62. Campioni, S., Mannini, B., Zampagni, M., Pensalfini, A., Parrini, C., Evangelisti, E., Relini, A., Stefani, M., Dobson, C. M., Cecchi, C., and Chiti, F. (2010) A causative link between the structure of aberrant protein oligomers and their toxicity. *Nat. Chem. Biol.* **6,** 140–147
63. Golde, T. E., Ran, Y., and Felsenstein, K. M. (2012) Shifting a complex debate on γ-secretase cleavage and Alzheimer disease. *EMBO J.* **31,** 2237–2239